Enhancing occupational heat risk preparedness through the integration of public weather forecasts and on-site observations

Yoojun Kim[1] and Youngjib Ham[1,2]

[1] Department of Construction Science, Texas A&M University, College Station, TX, USA
[2] yham@tamu.edu

Abstract. Heat exposure poses a significant threat to occupational safety, emphasizing the necessity of timely risk assessments to safeguard the workforce. Despite the critical role of heat risk assessment in occupational safety, its practical implementation is hindered by challenges in timely data collection, which impedes the deployment of proactive heat mitigation strategies. To bridge this information gap, this paper explores a methodological advancement designed to integrate public weather forecasts and on-site observations, enhancing the prediction and understanding of imminent occupational heat risks. We conducted a case study in College Station, Texas, as proof-of-concept. The case study confirms the performance improvements and identifies areas for further enhancement. This methodological advancement in heat risk assessment is to be of benefit to practitioners facilitating risk-informed decision-making for mitigating potential heat-related accidents in job sites.

Keywords: Occupational Safety, Heat Risk Forecasts, Proactive Management

1 Introduction

Although the increasing dangers of heat stress have been extensively documented in the occupational safety literature [1], gathering timely insights on when and to what extent heat stress impacts worker health and safety remains a challenge [2]. This issue becomes even more problematic when focusing on predicting future occupational heat risks, which are crucial for devising strategic preventive safety measures. Forecasting these risks necessitates the adoption of additional approaches, including data-driven predictive models, which are complex to implement alongside on-site measurement methods alone. The variability of weather conditions, which demands extensive numerical simulation and expert adjustment to account for global and local weather trends as well as daily and seasonal variations, further complicates understanding these risks at the workplace level.

In response to the need for predictive information on heat risk, the National Weather Service (NWS) began operating a Wet Bulb Globe Temperature (WBGT) forecast service (hereafter referred to as NWS WBGT forecasts) in June 2022 [3]. The WBGT index is extensively used for evaluating occupational heat risks [4]. These

public weather forecasting services offer great promise in bridging the information gap on imminent occupational heat risks by providing easily accessible forecasts without the need for additional effort. Recent evaluations [5,6] of their accuracy have shown NWS WBGT forecasts to exhibit a fidelity range from -0.64°C to 1.46°C [5]. Nevertheless, the broader implications of these forecasts for occupational safety management, beyond mere numerical accuracy, have yet to be fully explored, which is the primary focus of this study.

This study aims to enhance occupational safety by enhancing the utilization of public weather forecasts, integrating them with real-time weather conditions captured through on-site measurements. To achieve this, the research first evaluates the accuracy of public weather forecasts in predicting heat-related risks. It then explores the efficacy of an optimization approach that employs a Kalman filter to reduce forecast errors by incorporating on-site observational data. The research was conducted in College Station, Texas (30.6101° N, 96.3401° W), where forecast data and corresponding local observations are collected from May 1 to August 31, 2023, during the working hours of 7:00 to 20:00. The key contributions of this study are (1) practical insights into the effectiveness of the NWS WBGT forecast service and (2) enhancements to the accuracy of public forecasts using on-site observational data. The findings of this study are expected to advance our understanding of forthcoming heat risks that will help practitioners better mitigate occupational heat risks in jobsites.

2 Methods

2.1 Data Collection

The NWS WBGT forecast data are obtained from the National Digital Forecast Database (NDFD), which is publicly accessible through NOAA's website via both HTTP and FTP [7]. This dataset provides the NWS WBGT forecasts along with other weather forecasts, including air temperature (T_a), global horizontal irradiance (GHI), relative humidity (RH), and air velocity (V_a), with a forecast horizon set at 6 hours. Historical cloud cover data and dew point temperature are sourced from the High-Resolution Rapid Refresh (HRRR) model [8]. The sun’s zenith angle calculated by the SOLPOS algorithm [9]. On-site observation data are gathered from WeatherSTEM [10], encompassing hourly weather data such as T_a, RH, GHI, and V_a, which are essential for calculating observed WBGT values.

2.2 Data Processing

WBGT Calculation. The NWS WBGT computation mechanism utilizes a sequence of formulas to calculate the natural wet-bulb temperature (T_n) and black globe temperature (T_g). For T_n calculation, it initially determines the GHI using the Environment Canada weather forecast model [3], followed by the computation of T_n utilizing Equation (1):

$$T_n = T_w + 0.001651GHI - 0.09555V_a + 0.13235(T_a - T_w) + 0.20249 \quad (1)$$

where GHI is in W/m^2; V_a is in m/s; and T_a is in °C. For the computation of T_g, the algorithm primarily utilized is that proposed by [11], which necessitates the associated weather conditions for its calculation, including surface air pressure, dew point temperature, the sun's zenith angle, T_a, and GHI. The specifics of this computation mechanism are detailed in [3]. With T_n and T_g determined, the WBGT index is then calculated using Equation 2.

$$WBGT = 0.7T_n + 0.2T_g + 0.1T_a \quad (2)$$

Optimization with Kalman Filter. This study leverages the Kalman Filter to enhance the precision of WBGT forecasts. At its core, the Kalman Filter estimates the WBGT bias (i.e., the difference between the forecasted WBGT and the observed WBGT) by adjusting the initial state based on the calculated WBGT bias, considering the uncertainties of both the process and measurement. The estimation process initiates with an initialization phase, where the initial WBGT bias value is established as the initial state estimate. This is accompanied by an initial state covariance, set at a value of 1.0, to indicate the initial uncertainty level of the estimate. The procedure then moves forward by considering both process and measurement noise. The process noise, assumed to be 0.1, reflects the inherent variability in WBGT bias from one time step to the next, capturing natural fluctuations in environmental conditions. Concurrently, measurement noise, valued at 0.5 for the WBGT bias values, quantifies the expected inaccuracies within the measurement process. As the algorithm processes each hourly data point, it performs a series of prediction and update cycles. The prediction phase progresses the state estimate and its covariance from the prior time step to the current one, integrating process noise to manage the uncertainty in the state's development over time. This adjustment refines the state estimate and its uncertainty based on the measurement noise, utilizing the Kalman Gain to appropriately weigh the new WBGT bias estimate against the preceding prediction. This cyclical process of prediction and correction is executed for each hourly data point, resulting in a sequence of optimized WBGT estimates by amalgamating the updated WBGT bias estimate with the NWS WBGT forecast.

WBGT Heat Risk Levels. The evaluation of WBGT heat risk levels follows the guidelines proposed by the Armed Services [12], as detailed in Table 1. This set of criteria was selected by considering its practical applicability, which provides specific safety measures such as work/rest ratios and hydration guidelines [13]. This study explores the reliability of NWS WBGT forecasts in the context of employing these guidelines as reference criteria in safety management practices.

Table 1. Guidelines for work/rest ratios and water intake based on WBGT-based heat risk levels and work intensities.

Level	WBGT index (°C)	Easy work (250 W)		Moderate work (425 W)		Hard work (600 W)	
		Work/ Rest (min)	Water intake (qt·h-1)	Work/ Rest (min)	Water intake (qt·h-1)	Work/ Rest (min)	Water intake (qt·h-1)
1	25.6 ~ 27.7	Unlimited	0.5	Unlimited	0.75	40/20	0.75
2	27.8 ~ 29.4	Unlimited	0.5	50/10	0.75	30/30	1
3	29.4 ~ 31.1	Unlimited	0.75	40/20	0.75	30/30	1
4	31.1 ~ 32.2	Unlimited	0.75	30/30	0.75	20/40	1
5	32.2+	50/10	1	20/40	1	10/50	1

2.3 Data Analysis

The objective of this analysis is twofold: (1) to assess the accuracy of NWS WBGT forecasts and their practical implications in identifying heat risks, and (2) to assess the performance improvements achieved through Kalman filter-based optimization using on-site observations. The root mean squared error (RMSE) is employed as the main metric for assessing the accuracy of both the NWS WBGT forecasts and the enhanced forecasts. To evaluate the effectiveness in detecting heat risk levels, the F1 score is used to ensure a balanced assessment of precision and recall. Furthermore, to understand the impact of weather bias on detection efficacy, beta coefficients are calculated, which are the standardized coefficients in regression analysis.

3 Results and Discussion

3.1 Heat Risk Distribution in the Study Area

The climate of the study area is categorized under the humid subtropical climate type (Cfa) following the Köppen climate classification, which is prevalent in most southeastern areas of the United States [14]. Fig. 1(a) illustrates the distribution of WBGT heat risk levels, derived from on-site observed weather conditions. The distribution of heat risks spans across Level 1 (17.2%), Level 2 (17.6%), Level 3 (26.0%), Level 4 (16.3%), and Level 5 (7.7%). These variations are strongly associated with the time of day, especially during periods of heightened heat-related weather conditions, such as T_a or GHI, usually occurring post-noon, as shown in Fig. 1(b). The areas between the

first and third quantiles are marked in grey, while the black line graph depicts the mean WBGT values according to local hours. This underscores the temporal fluctuations in heat risk, emphasizing the critical periods, especially from 12:00 to 18:00, during which higher heat risk levels are observed. These periods align with increased variations in WBGT levels across the quantiles.

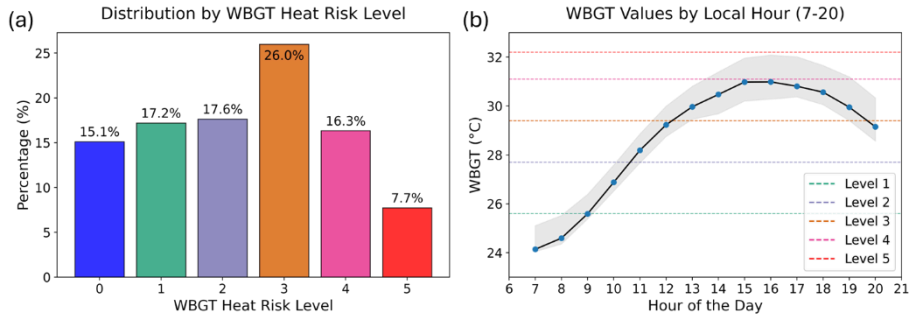

Fig. 1. (a) Distribution of WBGT heat risk levels as percentages in the study area; (b) Hourly mean WBGT values (7:00-20:00) with quantile ranges highlighted in grey.

3.2 Assessing NWS WBGT Forecasts and Kalman Filter Improvements

The blue line in Fig. 2(a) shows the hourly RMSE for NWS WBGT forecasts by local hour, ranging between 0.81℃ and 2.53℃, with an average of 1.58℃. This aligns with findings that the average RMSE is 1.7℃ for WBGT values above 26.7℃ and 1.5℃ for values above 29.4℃ in Chapel Hill, NC, also classified under the Cfa Köppen climate type [6]. Although this bias might seem acceptable for occupational heat risk assessments [5], its impact on occupational safety management requires more thorough investigation, as it may introduce inaccuracies in depicting occupational heat risk levels. Fig. 2(b) represents how this discrepancy affects different occupational heat risk levels, with all F1 scores under 0.5: Level 1 at 0.43, Level 2 at 0.24, Level 3 at 0.32, Level 4 at 0.28, and Level 5 at 0.34, suggesting its limited effectiveness as a decision-support tool for occupational heat risk management. On the other hand, the orange line in Fig. 2(a) depicts the hourly RMSE of NWS WBGT forecasts with Kalman filter adjustments by local hour, indicating an improvement in RMSE to between 0.58℃ and 1.14℃, with an average of 0.84℃. This adjustment results in higher F1 scores for identifying WBGT heat risk levels: 0.62 for Level 1, 0.58 for Level 2, 0.66 for Level 3, 0.33 for Level 4, and a decrease to 0.03 for Level 5, as illustrated in Fig. 2(c). The better performance in classifying levels 1-3 may be associated with the WBGT-based heat risk levels presented in Table 1, where the range for level 4 is narrower at 1.1℃, in comparison to the wider ranges for levels 1-3, which are 2.1℃, 1.6℃, and 1.7℃, respectively. Overall, the notable improvement in this preliminary study from applying the Kalman filter, an efficient and straightforward method, underscores its potential for refining public forecasts through data-driven post-processing that leverages on-site observations.

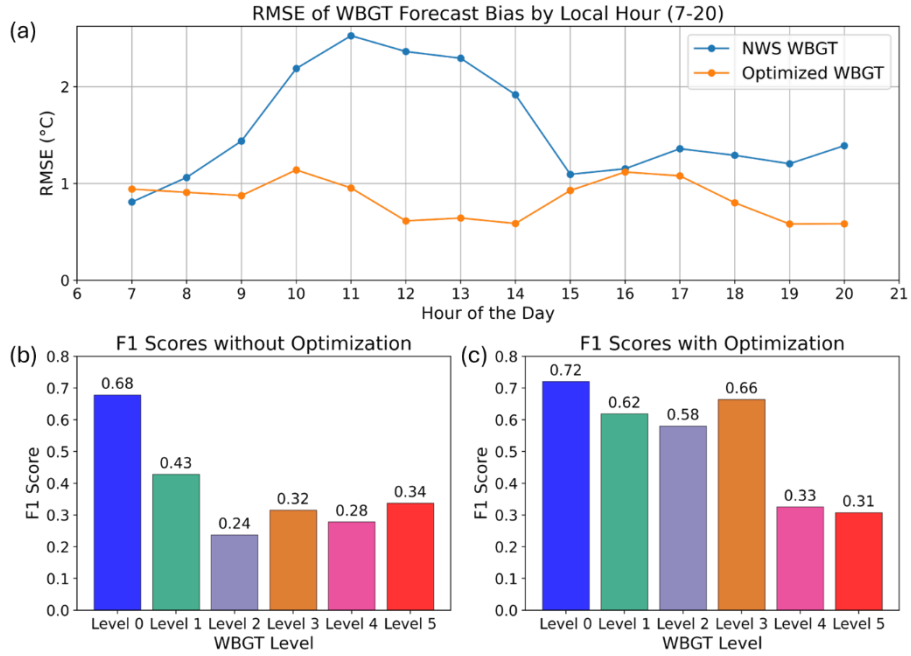

Fig. 2. (a) Hourly RMSE values (7:00-20:00) with/without optimization; (b) F1 scores for WBGT heat risk levels of NWS WBGT forecasts without Kalman filter optimization; (c) F1 scores for WBGT heat risk levels of NWS WBGT forecasts with Kalman filter optimization.

3.3 Heat Risk Forecast Misclassifications and Optimization Insights

We further explore the effectiveness of optimized heat risk forecasts to identify areas for future improvements. Fig. 3(a) illustrates a heatmap matrix showing the direct correlations between observed and forecasted WBGT risk levels following Kalman filter optimization. The data is normalized so that the sum of values within each row, representing an observed WBGT risk level, equals 100%. It is observed that misclassifications of heat risks tend to overestimate lower heat risk levels (Levels 0 to 2) and underestimate moderate to high heat risk levels (Levels 3 to 5 Furthermore, distinct misclassification trends are noted for Levels 4 and 5, often leading to estimations one level lower, such as forecasting Level 3 instead of Level 4 (72.9%, Case A) and Level 4 as Level 5 (60.7%, Case B). Figs. 3(b) and 3(c) elaborate on the beta coefficients for weather biases, including the differences between observed and forecasted variables in T_a (T_{a_diff}), RH ($RH_{\_diff}$), V_a (V_{a_diff}), and GHI ($GHI_{\_diff}$). T_{a_diff} is found to significantly affect WBGT bias, with $GHI_{\_diff}$ showing a more pronounced effect in Case B at 0.66. All coefficients have p-values below 0.05 and variance inflation factors (VIFs) below 4. These insights are instrumental for developing strategies to improve performance and optimize weather-specific performance, focusing on enhancing areas of weather forecast accuracy in the realm of occupational heat risk assessment.

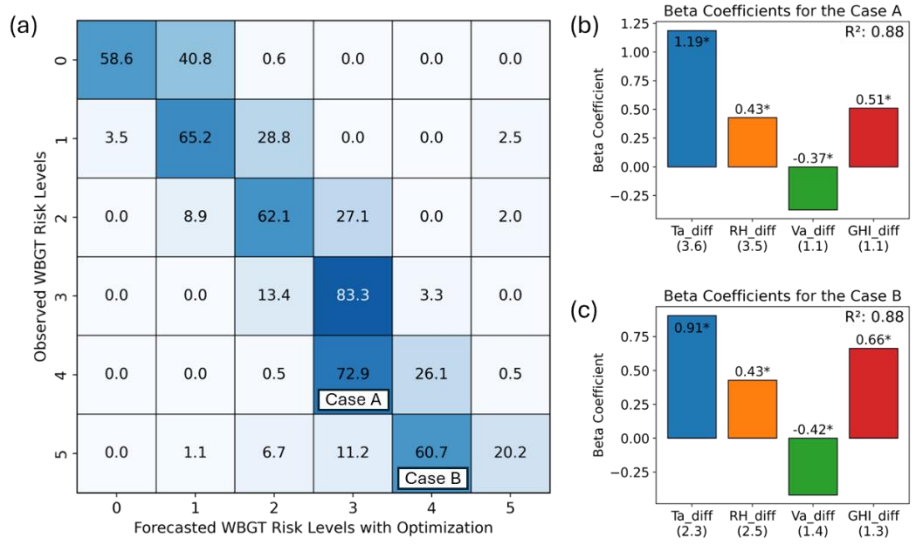

Fig. 3. (a) Analysis of WBGT risk level forecasts (a) Heatmap matrix of observed vs. optimized forecast levels; (b) Weather bias beta coefficients in misclassification of Level 4 as Level 3 (Case A); (c) Weather bias beta coefficients in misclassification of Level 5 as Level 4 (Case B).

4 Conclusion

Predictive insights into forthcoming heat risks are crucial for risk-informed occupational heat risk management. The NWS WBGT forecasts exhibit significant potential in offering such insights. This preliminary study, conducted during the summer of 2023 in College Station, TX, assesses the effectiveness of the NWS WBGT forecasts and develops an optimization strategy to enhance their accuracy with on-site weather observations. The main findings include: (1) NWS WBGT forecasts, while generally accurate with an average RMSE of 1.7°C, often misrepresent occupational heat risks, as shown by F1 scores below 0.5; (2) using a Kalman filter to minimize bias between observed and forecasted WBGT values enhances forecast precision; (3) such enhancements also improve heat risk level detection accuracy. Further exploration shows T_a and GHI biases significantly affect the underestimation of risk levels.

This study also identifies opportunities for further research and enhancements. Broadening the research scope to various climate types and forecasting horizons could deepen our understanding of the NWS forecasts' effectiveness. This expanded understanding could have practical implications for occupational safety management beyond the current preliminary results. Additionally, exploring other data-driven optimization techniques could yield additional performance enhancements, as demonstrated by the proposed Kalman filter-based optimization. In line with these insights, our continued research efforts focus on refining the heat risk forecast framework, aiming for more proactive and efficient heat risk assessments.

References

1. Ioannou L.G., Foster J., Morris N.B., Piil J.F., Havenith G., Mekjavic I.B., Kenny G.P., Nybo L., Flouris A.D., Occupational heat strain in outdoor workers: A comprehensive review and meta-analysis, Temperature 9, 67–102 (2022).
2. Kim Y., Ham Y., Revealing the Impact of Heat Radiation on Construction: A Microclimate Simulation Using Meteorological Data and Geometric Modeling, J. Constr. Eng. Manage 150 (2024).
3. Boyer T.R., NDFD Wet Bulb Globe Temperature Algorithm and Software Design, (2022), https://vlab.noaa.gov/documents/6609493/0/NDFD+WBGT+Description+Document.pdf, last accessed 2024/03/09.
4. Spangler K.R., Liang S., Wellenius G.A., Wet-Bulb Globe Temperature, Universal Thermal Climate Index, and Other Heat Metrics for US Counties, 2000–2020. Sci Data 9 (1) (2022).
5. Ahn Y., Uejio C.K., Rennie J., Schmit L., Verifying Experimental Wet Bulb Globe Temperature Hindcasts Across the United States, GeoHealth 6 (2022).
6. Clark J., Konrad C.E., Grundstein A., The Development and Accuracy Assessment of Wet Bulb Globe Temperature Forecasts, Weather and Forecasting 39, 403–419 (2024).
7. NOAA, National Digital Forecast Database (NDFD), (2023). https://vlab.noaa.gov/web/mdl/ndfd-grid-data, last accessed 2024/03/09.
8. NOAA, High-Resolution Rapid Refresh (HRRR), (2023). https://vlab.noaa.gov/web/mdl/nbm, last accessed 2024/03/09.
9. The National Renewable Energy Laboratory (NREL), NREL's Solar Position and Intensity (SOLPOS 2.0), (2001). https://www.nrel.gov/grid/solar-resource/solpos.html, last accessed 2024/03/09.
10. WeatherSTEM, WeatherSTEM (STEM), (2023). https://www.weatherstem.com, last accessed 2024/03/09.
11. Dimiceli V.E., Piltz S.F., Amburn S.A., Estimation of black globe temperature for calculation of the wet bulb globe temperature index, in: In Proceedings of the World Congress on Engineering and Computer Science 2011, San Francisco, US, (2011).
12. U.S. Department of Defense (DOD), Technical Manual NEHC-TM-OEM. 6260.6A, Prevention and Treatment of Heat and Cold Stress Injuries, (2007). https://www.med.navy.mil/Navy-and-Marine-Corps-Force-Health-Protection-Command/Environmental-Health/Occupational-and-Environmental-Medicine/Occupational-and-Environmental-Medicine-Division/Technical-Manuals-and-Guidance/, last accessed 2024/03/09.
13. Jacklitsch B., Williams W.J., Musolin K., Coca A., Kim J.-H., Turner N., Occupational exposure to heat and hot environments, Cincinnati: Dept. of Health and Human Services. (2016).
14. Chen D., Chen H.W., Using the Köppen classification to quantify climate variation and change: An example for 1901–2010, Environmental Development 6, 69–79 (2013).